Journal of Computational Physics 352 (2018) 445–462

Contents lists available at ScienceDirect

Journal of Computational Physics

www.elsevier.com/locate/jcp

Well-balanced discontinuous Galerkin methods with hydrostatic reconstruction for the Euler equations with gravitation

Gang Li [a,1], Yulong Xing [b,*,2]

[a] School of Mathematics and Statistics, Qingdao University, Qingdao, Shandong 266071, PR China
[b] Department of Mathematics, Ohio State University, Columbus, OH 43210, USA

ARTICLE INFO

Article history:
Received 7 February 2017
Received in revised form 2 September 2017
Accepted 30 September 2017
Available online 6 October 2017

Keywords:
Euler equations
Polytropic equilibrium
Discontinuous Galerkin methods
Well-balanced property
High order accuracy
Gravitational field

ABSTRACT

Many interesting astrophysical and atmospheric problems involve flows near the hydrostatic equilibrium state where the pressure gradient is balanced by the gravitational force. In this paper, we design high order well-balanced discontinuous Galerkin methods for the Euler equations with gravitation, which can preserve the discrete polytropic and isothermal hydrostatic balance states exactly. To achieve the well-balancedness, we propose to combine the numerical fluxes based on a generalized hydrostatic reconstruction, with an equilibrium state recovery technique and a novel source term approximation. Extensive one- and two-dimensional numerical examples are shown to demonstrate the performance of our well-balanced methods, and comparison with non-well-balanced results is included to illustrate the importance of maintaining the balance between pressure gradient and gravitational force numerically.

1. Introduction

In this paper, we design high order well-balanced discontinuous Galerkin (DG) methods for the solutions of the Euler equations with gravitation

$$\begin{aligned} &\rho_t + \nabla\cdot(\rho\mathbf{u}) = 0,\\ &(\rho\mathbf{u})_t + \nabla\cdot(\rho\mathbf{u}\otimes\mathbf{u} + p\mathbf{I}_d) = -\rho\nabla\phi,\\ &E_t + \nabla\cdot((E+p)\mathbf{u}) = -\rho\mathbf{u}\cdot\nabla\phi, \end{aligned} \tag{1.1}$$

that preserve their steady state solutions exactly in the discrete sense. Here $\mathbf{x}\in\mathcal{R}^d$ $(d=1,2,3)$ is the spatial variable, ρ, $\mathbf{u}$, p denote the fluid density, the velocity, and the pressure, respectively. $E=\frac{1}{2}\rho\|\mathbf{u}\|^2+\rho e$ (e is internal energy) is the non-gravitational energy which includes the kinetic and internal energy of the fluid. The operators ∇, $\nabla\cdot$ and $\otimes$ are the gradient, divergence and tensor product in $\mathcal{R}^d$, respectively, and $\mathbf{I}_d$ denotes the identity matrix. The source terms on the right hand side of the equations represent the effect of the gravitational force, and $\phi=\phi(\mathbf{x})$ is the time independent

* Corresponding author.
E-mail addresses: gangli1978@163.com (G. Li), xing.205@osu.edu (Y. Xing).
[1] The work of this author was partially supported by Natural Science Foundation of China (11201254, 11401332, 11771228).
[2] The work of this author was partially supported by the NSF grants DMS-1621111, DMS-1753581 and ONR grant N00014-16-1-2714.

https://doi.org/10.1016/j.jcp.2017.09.063
0021-9991/

gravitational potential. To close this system, the pressure p is linked to the density ρ and the interval energy e through an equation of state, denoted by $p = p(\rho, e)$. For example, the ideal gas law takes the form of

$$p = (\gamma - 1)\rho e = (\gamma - 1)\left(E - \rho\|\mathbf{u}\|^2/2\right), \tag{1.2}$$

where γ is the ratio of specific heats. This ideal gas law is used in the numerical examples section, but the methods presented in this paper are applicable beyond the ideal gas equation of state.

Euler equations under gravitational fields play an important role in modeling many interesting astrophysical and atmospheric phenomena, with examples including the simulation of supernova explosions, climate modeling and numerical weather forecasting. In these applications, we often encounter nearly steady state flows, which are small perturbation of the hydrostatic equilibrium states arising from the balance of the flux term and gravitational source term in (1.1). Two well-known hydrostatic equilibriums states of the Euler equations under gravitation are the isothermal and the polytropic equilibria, which will be explained in detail in Section 2. One computational challenge in simulating these nearly steady flows comes from the imbalance of numerical approximations to these terms, which will lead to truncation error that may be comparable with the size of the physical perturbation. As a result, the numerical solution may either oscillate around the equilibrium or deviate from the correct approximation. To resolve this problem, one may need to use an extremely refined mesh, which increases the computational cost and can become quite burdensome in multi-dimensional simulations. Well-balanced methods are designed to preserve these steady states solutions exactly up to the machine accuracy, and can effectively capture these small perturbations well even on relatively coarse meshes.

Study of well-balanced methods has attracted many attention in the past decade, and many well-balanced methods have been designed in the literature. Most of them are proposed for the shallow water equations over a non-flat bottom topology, which is another prototypical example of hyperbolic conservation laws with source term. We refer the readers to [2,12,1,15, 21,31,26,30,29] and the references therein for some limited references in this context. Recently, some of these approaches have been extended to design well-balanced numerical methods for the Euler equations with gravitation. An early work can be found in [16], where the quasi-steady wave-propagation methods are applied to the Euler equations. Later, finite volume well-balanced methods have been proposed in [3] for the nearly hydrostatic flows in the numerical weather prediction. Gas-kinetic schemes have been extended to the multidimensional gas dynamic equations in [24,32,19], and well-balanced numerical methods were developed. Finite volume well-balanced schemes for the general hydrostatic equilibrium without any assumption of a thermal equilibrium are recently studied in [13,14]. Other related work can be found in [33,10,6]. The first high order version of well-balanced methods for the isothermal equilibrium of the Euler equations with gravitation is introduced in [28], based on a reformulation of the source term and a slightly modified weighted essentially non-oscillatory (WENO) reconstruction operator. The well-balanced approach based on reformulating the source term has been extended to DG methods in [17], to the nodal DG methods in [7], to the compact-reconstruction WENO methods for atmospheric flows in [11], and to the finite volume WENO methods in [18].

Another popular approach in designing well-balanced methods for the shallow-water equations is the hydrostatic reconstruction idea, first proposed in [1] and later appearing in many well-balanced methods including some high order ones. Numerical flux based on hydrostatic reconstruction, combined with novel well-balanced source term approximation, is an important idea in designing well-balanced DG methods for the lake at rest steady state [27,30], and for the general moving equilibrium state of the shallow water equations [4,5,25]. In this paper, we plan to extend the hydrostatic reconstruction idea to investigate novel well-balanced DG methods for the polytropic equilibrium of the Euler equations with gravitation, which appears in most of these astrophysical applications. Their extension to the isothermal equilibrium state will also be described. Our well-balanced DG methods are build upon the first order methods in [13]. In [13], second order extension has also been presented, and our methods can be viewed as their extension to arbitrary high order methods in the DG setting. To achieve the well-balancedness, we proposed to combine the numerical fluxes based on hydrostatic reconstruction, with the equilibrium state recovery technique and a novel source term approximation. The proposed DG methods can also be viewed as a generalization of the methods designed for balancing the shallow water equations with moving water equilibrium in [25], and are very different from the existing two well-balanced DG methods in [17,7].

This paper is organized as follows. In Section 2, we present the one dimensional model and its steady state solutions. In Sections 3 and 4, our well-balanced DG methods for the polytropic hydrostatic steady states of the Euler equations under gravitational filed are presented. We start with one dimensional problem, and then extend the proposed method to multi-dimensional case. Section 5 contains extensive numerical simulation results to demonstrate the behavior of our well-balanced DG methods for one- and two-dimensional Euler equations under gravitational field, verifying high order accuracy, the well-balanced property, and good resolution for smooth and discontinuous solutions. Some conclusions are given in Section 6.

2. Mathematical model

In one spatial dimension, the Euler equations (1.1) reduce to the form of

$$\begin{aligned} &\rho_t + (\rho u)_x = 0, \\ &(\rho u)_t + (\rho u^2 + p)_x = -\rho\phi_x, \\ &E_t + ((E + p)u)_x = -\rho u\phi_x, \end{aligned} \tag{2.1}$$

governing the conservation of mass, momentum and energy. Here u is the one dimensional velocity. This model admits the hydrostatic stationary solution, where the pressure gradient force is balanced by the external forces such as gravity:

$$\rho = \rho(x), \quad u = 0, \quad p_x = -\rho\phi_x. \tag{2.2}$$

As explained in [13], such relation alone is not complete, and the pressure stratifications are not uniquely defined. One usually needs to specify the profile of another variable, usually the temperature or entropy, to determine the stable equilibrium. Two important special equilibria arising in the applications are the isothermal (constant temperature) [28] and polytropic (constant entropy) hydrostatic equilibrium states [13].

For an ideal gas satisfying

$$p(x) = \rho(x)RT(x), \tag{2.3}$$

with R being the gas constant, we can integrate the steady state solution (2.2) and obtain

$$\rho = \frac{p_0}{RT(x)} \exp\left(-\int_{x_0}^{x} \frac{\phi_x(s)}{RT(s)} ds\right), \qquad u = 0, \qquad p = p_0 \exp\left(-\int_{x_0}^{x} \frac{\phi_x(s)}{RT(s)} ds\right), \tag{2.4}$$

where p_0 is the initial pressure at some reference position x_0. For the isothermal equilibrium state, the temperature $T(x) \equiv T_0$ becomes a constant, and the equilibrium correspondingly becomes

$$\rho = \rho_0 \exp\left(-\frac{\phi}{RT_0}\right), \qquad u = 0, \qquad p = p_0 \exp\left(-\frac{\phi}{RT_0}\right), \tag{2.5}$$

with $p_0 = \rho_0 RT_0$.

The other polytropic hydrostatic equilibrium, which appears frequently in the astrophysical applications and is the focus of this paper, is characterized by

$$p = K\rho^{\gamma}, \tag{2.6}$$

which will lead to the form of

$$\rho = \left(\frac{\gamma - 1}{K\gamma}(C - \phi)\right)^{\frac{1}{\gamma-1}}, \qquad u = 0, \qquad p = \frac{1}{K^{\frac{1}{\gamma-1}}}\left(\frac{\gamma - 1}{\gamma}(C - \phi)\right)^{\frac{\gamma}{\gamma-1}}, \tag{2.7}$$

where C and K are both constants. As shown in [13], an equivalent formulation of (2.7) is given by

$$u = 0, \quad h + \phi = C, \tag{2.8}$$

where $h = e + p/\rho$ denotes the specific enthalpy. The equilibrium (2.8) is obtained from the thermodynamics relation $\mathrm{d}h = T\mathrm{d}s + \mathrm{d}p/\rho$. In the case of constant entropy, we have $\mathrm{d}s \equiv 0$, therefore $\mathrm{d}h = \mathrm{d}p/\rho = -\mathrm{d}\phi$, namely $\mathrm{d}(h + \phi) = 0$, which consequently leads to (2.8). The equilibrium state (2.7) can now be rewritten as

$$\rho = \left(\frac{\gamma - 1}{K\gamma}h\right)^{\frac{1}{\gamma-1}}, \qquad u = 0, \qquad p = \frac{1}{K^{\frac{1}{\gamma-1}}}\left(\frac{\gamma - 1}{\gamma}h\right)^{\frac{\gamma}{\gamma-1}}. \tag{2.9}$$

The simplest gravity encountered is the linear gravitational potential field with $\phi_x = g$, and the corresponding polytropic hydrostatic balance takes the form of

$$p = p_0^{\frac{1}{\gamma-1}}\left(p_0 - \frac{\gamma - 1}{\gamma} g\rho_0 x\right)^{\frac{\gamma}{\gamma-1}}, \qquad u = 0, \qquad \rho = \rho_0\left(\frac{p}{p_0}\right)^{\frac{1}{\gamma}}. \tag{2.10}$$

3. Well-balanced DG methods for one dimensional problem

In this section, we present high order well-balanced DG methods for the Euler equations with gravity, with the objective to maintain the polytropic steady state solution (2.8) and the isothermal steady state solution (2.5). We will concentrate on the one-dimensional case in this section, and discuss the generalization to high dimensional case in the next section.

3.1. Notations

We start by presenting some standard notations to be used later in the paper. The interval $I = [a, b]$ is divided into N subintervals and we denote the cells by $I_j = [x_{j-\frac{1}{2}}, x_{j+\frac{1}{2}}]$ for $j = 1, \cdots, N$. The center of each cell is $x_j = \frac{1}{2}(x_{j-\frac{1}{2}} + x_{j+\frac{1}{2}})$, and the mesh size is denoted by $\tau_j = x_{j+\frac{1}{2}} - x_{j-\frac{1}{2}}$, with $\tau = \max_{1\le j\le N} \tau_j$ being the maximal mesh size. The piecewise polynomial space V_τ^k is defined as the space of polynomials of degree up to k in each cell I_j:

$$V_\tau^k = \left\{ v : v|_{I_j} \in P^k(I_j),\ j = 1, 2, \cdots, N \right\}. \tag{3.1}$$

Note that the functions in V_τ^k are allowed to have discontinuities across element interfaces.

Following the standard DG notation, for any unknown variable u, its numerical approximation in the DG methods is denoted by u_τ, which belongs to the finite element space V_τ^k. We denote by $u^+_{\tau,j+\frac{1}{2}}$ and $u^-_{\tau,j+\frac{1}{2}}$ the limit values of u_τ at $x_{j+\frac{1}{2}}$ from the right cell I_{j+1} and from the left cell I_j, respectively.

For the sake of easy presentation, we introduce the following notations:

$$U = \begin{pmatrix} \rho \\ \rho u \\ E \end{pmatrix}, \quad V = \begin{pmatrix} \rho \\ u \\ p \end{pmatrix}, \tag{3.2}$$

to denote the conservative and the primitive variables, respectively. The Euler equations with gravitation (2.1) are re-written as

$$U_t + F(U)_x = S(U, \phi), \tag{3.3}$$

where $F(U)$ and $S(U, \phi)$ denote the flux and source term, respectively.

3.2. Recovery of the well-balanced states

The first difficulty in designing well-balanced DG methods is the recovery of well-balanced states from the initial condition, provided as a piecewise polynomial in V_τ^k. Let's assume that the initial data $U(x, t = 0) = U_0(x)$ are in a perfect equilibrium state, i.e.,

$$u = 0, \quad h + \phi = \text{constant C}, \tag{3.4}$$

where $h = h(U_0(x)) = e + p/\rho$ can be computed from the variables U_0. Usually, we take the L^2 projection of U_0 to be the initial condition of the DG methods. However, the projected polynomial, denoted by $U_{0,\tau}$, may not be in the equilibrium state. Therefore, the cell boundary values $U^\pm_{\tau,j+\frac{1}{2}}$, which will be used to evaluate the numerical fluxes, may not be in equilibrium, and this will increase the complexity in designing well-balanced methods. The same difficulty has been observed when designing well-balanced methods for the shallow water equation with moving water equilibrium state. In [20,25], we define the initial condition of equilibrium variables as the solution of a nonlinear equation and solve it by Newton's iteration. Such approach can also be extended here, but it is rather complicated.

In this paper, we propose a different approach to recover the well-balanced states. The initial condition of DG methods can be any polynomial which approximates the exact solution and at the same time has enough accuracy. We introduce a new projection of the initial condition by defining $\mathbb{P}_\tau^c \omega$ to be a projection of ω into V_τ^k, such that

$$\int_{I_j} \mathbb{P}_\tau^c \omega v \, dx = \int_{I_j} \omega v \, dx,$$

for any $v \in P^{k-1}$ on I_j, and

$$(\mathbb{P}_\tau^c \omega)(x_j) = \omega(x_j), \quad \text{at the center } x_j \text{ of the cell } I_j.$$

The polynomial $\mathbb{P}_\tau^c \omega$ on each cell I_j can be obtained by solving a linear algebra problem of size $(k+1) \times (k+1)$ locally. It is easy to show [8] the optimal convergence of this projection:

$$\|\omega^e\| + \tau \|\omega^e\|_\infty + \tau^{\frac{1}{2}} \|\omega^e\|_{\Gamma_\tau} \le C \tau^{k+1}, \tag{3.5}$$

where $\omega^e = \omega - \mathbb{P}_\tau^c \omega$ and Γ_τ denotes the set of boundary points of all cells. The constant C depends on the function ω, but is independent of the mesh size τ.

We define the initial condition $U_{0,\tau}$, and the projection of gravitational potential $\phi_\tau(x)$, to be

$$U_{0,\tau}(x) = \mathbb{P}_\tau^c U_0(x), \qquad \phi_\tau(x) = \mathbb{P}_\tau^c \phi(x). \tag{3.6}$$

In addition to optimal convergence of the projection $\mathbb{P}_\tau^c$, we can show that

$$U_{0,\tau}(x_j) = U_0(x_j), \qquad \phi_\tau(x_j) = \phi(x_j), \qquad \text{for all } j,$$

which leads to

$$h(p_\tau(x_j),\ \rho_\tau(x_j)) + \phi_\tau(x_j) = h(p(x_j),\ \rho(x_j)) + \phi(x_j) = C, \qquad \text{for all } j. \tag{3.7}$$

Therefore, at the center of each cell, we have recovered the equilibrium state (3.4), which now holds for the piecewise polynomials $U_{0,\tau}$ and ϕ_τ, the projection of the exact initial conditions. Note that even the initial condition is in the perfect equilibrium, such relation is only true for the numerical initial condition at the point x_j within each cell I_j.

Next, we propose to decompose the solution U_τ into the reference equilibrium state U_τ^e and the remaining part U_τ^r. This is one of the key ideas in designing the well-balanced methods, and will be applied to not only the initial condition but also the solution at each time step. To compute U_τ^e, we first define the equilibrium component of the specific enthalpy $h^e(x)$ as

$$h^e(x) = h(p_\tau(x_j),\ \rho_\tau(x_j)) + \phi_\tau(x_j) - \phi(x). \tag{3.8}$$

From the equilibrium state of the form (2.9), we can obtain the equilibrium component of the density, velocity, and pressure as follows:

$$\begin{aligned} \rho^e(x) &= \left(\frac{1}{K}\frac{\gamma-1}{\gamma}h^e(x)\right)^{\frac{1}{\gamma-1}}, \\ p^e(x) &= \left(\frac{1}{K}\right)^{\frac{1}{\gamma-1}}\left(\frac{\gamma-1}{\gamma}h^e(x)\right)^{\frac{\gamma}{\gamma-1}}, \\ u^e(x) &= 0, \end{aligned} \tag{3.9}$$

where K can be simply evaluated by $K_j = p_\tau(x_j)/\rho_\tau(x_j)^\gamma$ in the cell I_j. We denote them by

$$V^e(x) = \left(\rho^e(x),\ u^e(x),\ p^e(x)\right)^T := V^e(h^e(x)), \tag{3.10}$$

and can compute the equilibrium functions $U^e(x) = U(V^e(x))$ from (3.2). Since they may not be polynomials, we now project them into the piecewise polynomial space V_τ^k using the same projection $\mathbb{P}_\tau^c$, and denote the resulting functions by

$$U_\tau^e(x) = \mathbb{P}_\tau^c U^e = \mathbb{P}_\tau^c U(V^e(x)). \tag{3.11}$$

Therefore, we can decompose the numerical solutions U_τ as follows:

$$U_\tau = U_\tau^e + U_\tau^r, \tag{3.12}$$

where $U_\tau^r = U_\tau - U_\tau^e \in V_\tau^k$. Both U_τ^e and U_τ^r will be used exclusively during the construction of well-balanced fluxes and source term approximation.

Remark 1. If the initial condition is the equilibrium state (3.4), the numerical initial condition $U_{0,\tau}$ is then given by the projection $\mathbb{P}_\tau^c$ in (3.6). Based on the procedure above, we know that $h^e(x)$ recovers the exact specific enthalpy $h(x)$ by (3.7). Therefore, $V^e(x)$ is exactly the initial condition, and the equilibrium component $U_{0,\tau}^e$ is the same as $U_{0,\tau}$. So we have $U_{0,\tau}^r = 0$ in this case.

Remark 2. We would like to comment that the choice of the projection $\mathbb{P}_\tau^c$ is not unique. Instead of requiring the projected function matches the original function at the cell center x_j, we can choose any other point y_j within the cell I_j, with the relation (3.7) now holding at the point y_j. The standard L^2 projection is another popular choice to define the initial condition of DG methods. Although we cannot prove (3.7) theoretically when L^2 projection is used, we have tested it numerically and noticed that the error is relatively small (around 10^{-14}) when quadratic polynomial (i.e., $k = 2$) is used.

3.3. Well-balanced numerical fluxes

The standard DG methods for the equations (3.3) are given by

$$\int_{I_j} (U_\tau)_t v\,dx - \int_{I_j} F(U_\tau) v_x dx + \widehat{F}_{j+\frac{1}{2}} v(x_{j+\frac{1}{2}}^-) - \widehat{F}_{j-\frac{1}{2}} v(x_{j-\frac{1}{2}}^+) = \int_{I_j} S v\,dx, \tag{3.13}$$

where $v(x)$ is a test function in the test space V_τ^k, and $\widehat{F}_{j\pm1/2}$ are the numerical flux. A well-balanced DG method for the isothermal equilibrium state of the Euler equation has been designed in [17] using this formulation and a novel source term reformulation. Here, we would like to follow a different approach by utilizing the hydrostatic reconstruction idea in the

numerical flux. Such well-balanced DG methods for the shallow water equations have been studied in [27,30,25]. Following the setup in those papers, the semi-discrete well-balanced DG methods for (3.3) are defined as follows: for any test function $v(x) \in V_\tau^k$, U_τ is given by

$$\int_{I_j} (U_\tau)_t v \mathrm{d}x - \int_{I_j} F(U_\tau) v_x \mathrm{d}x + \widehat{F}^l_{j+\frac{1}{2}} v(x^-_{j+\frac{1}{2}}) - \widehat{F}^r_{j-\frac{1}{2}} v(x^+_{j-\frac{1}{2}}) = \int_{I_j} S v \mathrm{d}x, \tag{3.14}$$

or equivalently,

$$\begin{aligned} &\int_{I_j} (U_\tau)_t v \mathrm{d}x - \int_{I_j} F(U_\tau) v_x \mathrm{d}x + \widehat{F}_{j+\frac{1}{2}} v(x^-_{j+\frac{1}{2}}) - \widehat{F}_{j-\frac{1}{2}} v(x^+_{j-\frac{1}{2}}) \\ &\quad = \int_{I_j} S v \mathrm{d}x + \left(\widehat{F}_{j+\frac{1}{2}} - \widehat{F}^l_{j+\frac{1}{2}}\right) v(x^-_{j+\frac{1}{2}}) - \left(\widehat{F}_{j-\frac{1}{2}} - \widehat{F}^r_{j-\frac{1}{2}}\right) v(x^+_{j-\frac{1}{2}}), \end{aligned} \tag{3.15}$$

where the numerical fluxes $\widehat{F}^l_{j+\frac{1}{2}}$ and $\widehat{F}^r_{j-\frac{1}{2}}$ are computed based on hydrostatic reconstruction idea and will be defined in (3.17) below. The left side of (3.15) is the traditional DG method, and the right side can be viewed as our approximation to the source term. We point out here that $\widehat{F}_{j+\frac{1}{2}} - \widehat{F}^l_{j+\frac{1}{2}}$ and $\widehat{F}_{j-\frac{1}{2}} - \widehat{F}^r_{j-\frac{1}{2}}$ are both high order correction terms at the level of $O(\triangle x^{k+1})$ regardless of the smoothness of the solution U.

At each time step t^n, the cell boundary values $U^\pm_{\tau,j+\frac{1}{2}}$ can be computed from the piecewise polynomial solution $U_\tau(x)$ directly. However, in the case of equilibrium state, these cell boundary values do not equal the exact solution values at the same point even $U_\tau(x)$ are computed from the exact equilibrium, because the projection does not preserve the equilibrium state at two cell boundary points. To overcome this problem, we redefine an updated boundary value as:

$$\begin{aligned} U^{*,-}_{\tau,j+\frac{1}{2}} &= U\left(V^e\left(h(p_\tau(x_j),\ \rho_\tau(x_j)) + \phi_\tau(x_j) - \phi^*_{\tau,j+\frac{1}{2}}\right)\right) + U^{r,-}_{\tau,j+\frac{1}{2}}, \\ U^{*,+}_{\tau,j-\frac{1}{2}} &= U\left(V^e\left(h(p_\tau(x_j),\ \rho_\tau(x_j)) + \phi_\tau(x_j) - \phi^*_{\tau,j-\frac{1}{2}}\right)\right) + U^{r,+}_{\tau,j-\frac{1}{2}}, \end{aligned} \tag{3.16}$$

where

$$\phi^*_{\tau,j+\frac{1}{2}} = \max\left(\phi^-_{\tau,j+\frac{1}{2}},\ \phi^+_{\tau,j+\frac{1}{2}}\right), \qquad \text{for all } j,$$

and

$$U^{r,-}_{\tau,j+\frac{1}{2}} = U^r_\tau(x^-_{j+\frac{1}{2}}), \qquad U^{r,+}_{\tau,j-\frac{1}{2}} = U^r_\tau(x^+_{j-\frac{1}{2}}).$$

Here, the function $V^e(\cdot)$ is presented in (3.10) and U^r_τ is defined in (3.12). In the case of equilibrium state, we have $U^{r,\pm}_{\tau,j+\frac{1}{2}} = 0$, and $h(p_\tau(x_j),\ \rho_\tau(x_j)) + \phi_\tau(x_j) \equiv C$ from (3.7), therefore, $U^{*,+}_{\tau,j+\frac{1}{2}} = U^{*,-}_{\tau,j+\frac{1}{2}}$ for all j.

Next, we define the well-balanced numerical fluxes in (3.14) as follows:

$$\begin{aligned} \widehat{F}^l_{j+\frac{1}{2}} &= f\left(U^{*,-}_{\tau,j+\frac{1}{2}},\ U^{*,+}_{\tau,j+\frac{1}{2}}\right) + F\left(U^-_{\tau,j+\frac{1}{2}}\right) - F\left(U^{*,-}_{\tau,j+\frac{1}{2}}\right), \\ \widehat{F}^r_{j-\frac{1}{2}} &= f\left(U^{*,-}_{\tau,j-\frac{1}{2}},\ U^{*,+}_{\tau,j-\frac{1}{2}}\right) + F\left(U^+_{\tau,j-\frac{1}{2}}\right) - F\left(U^{*,+}_{\tau,j-\frac{1}{2}}\right), \end{aligned} \tag{3.17}$$

where $f(a_1, a_2)$ is a numerical flux. For example, we could use the simple Lax–Friedrichs flux

$$f(a_1, a_2) = \frac{1}{2}(F(a_1) + F(a_2) - \alpha(a_2 - a_1)), \tag{3.18}$$

where $\alpha = \max_x |\lambda(U)|$ with $\lambda(U)$ being the eigenvalues of the Jacobian $F'(U)$, and the maximum is taken over the whole region. When the condition $U^{*,+}_{\tau,j+\frac{1}{2}} = U^{*,-}_{\tau,j+\frac{1}{2}}$ holds, we can easily observe that $\widehat{F}^l_{j+\frac{1}{2}} = F\left(U^-_{\tau,j+\frac{1}{2}}\right)$ and $\widehat{F}^r_{j-\frac{1}{2}} = F\left(U^+_{\tau,j-\frac{1}{2}}\right)$ from the consistency of the numerical flux $f(a_1, a_2)$.

3.4. The source term approximation

To approximate the source term $\int_{I_j} S(U_\tau, \phi_\tau) v \, dx$, we first use the decomposition of U_τ in (3.12) to rewrite it as

$$\int_{I_j} S(U_\tau, \phi_\tau) v \, dx = \int_{I_j} S(U^e_\tau, \phi_\tau) v \, dx + \int_{I_j} S(U^r_\tau, \phi_\tau) v \, dx, \tag{3.19}$$

since the source terms $-\rho\phi_x$ and $-\rho u\phi_x$ in (2.1) are linear with respect to ρ and ρu.

The second term on the right hand side of (3.19) can be computed by the Gaussian quadrature rule directly. Here we discuss the numerical procedures for the first term only. Using the fact that U^e is the equilibrium state, we have the relation

$$\int_{I_j} S(U^e, \phi) v \, dx = -\int_{I_j} F(U^e) v_x \, dx + F(U^{e,-}_{j-\frac{1}{2}}) v(x^-_{j+\frac{1}{2}}) - F(U^{e,+}_{j-\frac{1}{2}}) v(x^+_{j-\frac{1}{2}}). \tag{3.20}$$

Since $U^e_\tau = \mathbb{P}^c_\tau U^e$, ϕ_τ are the projection of U^e and ϕ, we obtain that

$$\int_{I_j} S(U^e_\tau, \phi_\tau) v \, dx + \mathcal{O}(\tau^{k+1}) = -\int_{I_j} F(U^e_\tau) v_x \, dx + F(U^{e,-}_{\tau,j-\frac{1}{2}}) v(x^-_{j+\frac{1}{2}}) - F(U^{e,+}_{\tau,j-\frac{1}{2}}) v(x^+_{j-\frac{1}{2}}). \tag{3.21}$$

Therefore, the source term (3.19) can be approximated by

$$\int_{I_j} S(U_\tau, \phi_\tau) v \, dx \approx -\int_{I_j} F(U^e_\tau) v_x \, dx + F(U^{e,-}_{\tau,j-\frac{1}{2}}) v(x^-_{j+\frac{1}{2}}) - F(U^{e,+}_{\tau,j-\frac{1}{2}}) v(x^+_{j-\frac{1}{2}}) + \int_{I_j} S(U^r_\tau, \phi_\tau) v \, dx. \tag{3.22}$$

For the source term $-\int_{I_j} (\rho u)_\tau (\phi_\tau)_x v \, dx$ which becomes zero at the equilibrium state, we can also apply the Gaussian quadrature rule with enough accuracy directly. The approximation to the other source term takes the form of

$$\begin{aligned} -\int_{I_j} \rho_\tau (\phi_\tau)_x v \, dx \approx & \left(\rho^e_\tau (u^e_\tau)^2 + p^e_\tau\right)^-_{j+\frac{1}{2}} v(x^-_{j+\frac{1}{2}}) - \left(\rho^e_\tau (u^e_\tau)^2 + p^e_\tau\right)^+_{j-\frac{1}{2}} v(x^+_{j-\frac{1}{2}}) \\ & - \int_{I_j} \left(\rho^e_\tau (u^e_\tau)^2 + p^e_\tau\right) v_x \, dx - \int_{I_j} \rho^r_\tau (\phi_\tau)_x v \, dx \\ = & \, p^{e,-}_{\tau,j+\frac{1}{2}} v(x^-_{j+\frac{1}{2}}) - p^{e,+}_{\tau,j-\frac{1}{2}} v(x^+_{j-\frac{1}{2}}) - \int_{I_j} p^e_\tau v_x \, dx - \int_{I_j} \rho^r_\tau (\phi_\tau)_x v \, dx, \end{aligned} \tag{3.23}$$

due to the approximation (3.22) and the fact that $u^e_\tau = 0$.

3.5. Summary of the well-balanced DG methods

We now summarize the complete procedure of our high order well-balanced DG methods for solving the Euler equations (2.1) with the polytropic equilibrium (2.9). The numerical methods are given by (3.14), with the numerical fluxes $\widehat{F}^l$ and $\widehat{F}^r$ computed in (3.17), and the source term approximated by (3.22) or (3.23). The method is completed by combining with high order total variation diminishing (TVD) Runge–Kutta methods [23]. In the numerical section of this paper, we apply the following third order Runge–Kutta methods:

$$\begin{aligned} U^{(1)} &= U^n + \Delta t \mathcal{F}(U^n) \\ U^{(2)} &= \frac{3}{4} U^n + \frac{1}{4}\left(U^{(1)} + \Delta t \mathcal{F}(U^{(1)})\right) \\ U^{n+1} &= \frac{1}{3} U^n + \frac{2}{3}\left(U^{(2)} + \Delta t \mathcal{F}(U^{(2)})\right), \end{aligned} \tag{3.24}$$

with $\mathcal{F}(U)$ being the spatial operator.

Slope limiter procedure is usually needed for the hyperbolic conservation laws when the solution may contain discontinuities. The total variation bounded (TVB) limiter [9,22] is used in this paper. However, the standard TVB limiter procedure may violate the exact preservation of the steady state solution, and destroy the well-balanced property. Here we propose the following well-balanced way to perform the TVB limiter. In each cell I_j, the DG solution U_τ is separated as the sum of two

polynomials U_τ^e and U_τ^r, where U_τ^e is the projection of the equilibrium component of the solution. Since the equilibrium state does not contain any discontinuity, we can focus on the U_τ^r in the slope limiter procedure. Therefore, we proposed to apply the TVB slope limiter on the polynomials U_τ^r only, and then add U_τ^e back to obtain the limited solution U_τ. When the limiting procedure is implemented this way, if the steady state is reached, $U_\tau^r = 0$, hence we do not apply any TVB limiter. Therefore the well-balanced property is maintained.

A detailed implementation of this algorithm consists of the following steps:

1. Compute the projection of U_0 and the gravitational potential function ϕ based on the given initial data, and denote them by $U_{0,\tau}$ and ϕ_τ.
2. At each time step, compute the reference value V^e from (3.9)–(3.10), and decompose the solution U_τ as the sum of U_τ^e and U_τ^r following (3.11)–(3.12).
3. Compute the well-balanced numerical fluxes following the hydrostatic reconstruction idea in (3.16)–(3.18).
4. Evaluate the source term approximation by (3.22) or (3.23), as well as the Gaussian quadrature rule.
5. Apply the TVD Runge–Kutta method (3.24) to advance in time, implement the updated slope limiter procedure, and repeat steps 2–5.

All these together lead to a well-balanced DG method for the Euler equations with the polytropic hydrostatic balance under the gravitational field, as outlined in the following proposition.

Proposition 3.1. *For the Euler equations (2.1) under the gravitational field, the semi-discrete DG methods (3.14), combined with (3.17) and (3.22), are well-balanced for the steady state solution (2.9).*

Proof. Suppose that the initial data are the polytropic steady state. Easy to observe that the well-balanced property holds for the first and third equations, as both the flux and source term approximations in these equations become zero. We only need to show that the numerical approximations to the flux and source term of the second momentum equation cancel exactly.

By the construction of U_τ^e, we can show that U_τ^e is equivalent to U_τ and $U_\tau^r = 0$ in (3.12). Therefore the source term approximation (3.22) becomes

$$\begin{aligned}\int_{I_j} S(U_\tau, \phi_\tau) v \, dx &= -\int_{I_j} F(U_\tau^e) v_x \, dx + F(U^{e,-}_{\tau,j-\frac{1}{2}}) v(x^-_{j+\frac{1}{2}}) - F(U^{e,+}_{\tau,j-\frac{1}{2}}) v(x^+_{j-\frac{1}{2}}) \\ &= -\int_{I_j} F(U_\tau) v_x \, dx + F(U^-_{\tau,j-\frac{1}{2}}) v(x^-_{j+\frac{1}{2}}) - F(U^+_{\tau,j-\frac{1}{2}}) v(x^+_{j-\frac{1}{2}}). \end{aligned} \tag{3.25}$$

For the numerical fluxes, we have $U^{r,\pm}_{\tau,j+\frac{1}{2}} = 0$, and therefore, $U^{*,+}_{\tau,j+\frac{1}{2}} = U^{*,-}_{\tau,j+\frac{1}{2}}$ from the calculation in (3.16). The consistency property of numerical flux F in (3.17) leads to

$$\widehat{F}^l_{j+\frac{1}{2}} = F\left(U^-_{\tau,j+\frac{1}{2}}\right), \quad \widehat{F}^r_{j-\frac{1}{2}} = F\left(U^+_{\tau,j-\frac{1}{2}}\right), \tag{3.26}$$

and the approximation of the flux terms on the left hand side of (3.14) becomes

$$-\int_{I_j} F(U_\tau) v_x \, dx + F(U^-_{\tau,j-\frac{1}{2}}) v(x^-_{j+\frac{1}{2}}) - F(U^+_{\tau,j-\frac{1}{2}}) v(x^+_{j-\frac{1}{2}}),$$

which is exactly the same as the source term approximation in (3.25). Therefore, we can conclude that the proposed methods achieve the desired well-balanced property. □

Remark 3. If there is no gravitation field, i.e., $\phi_x = 0$, our well-balanced DG methods become the traditional DG methods. Also, the first order version of our well-balanced methods reduces to the one presented by Käppeli and Mishra in [13].

3.6. Well-balanced methods for the isothermal equilibrium

The well-balanced methods described above are designed for the polytropic equilibrium (2.8), but the same methodology can be easily applied to the isothermal equilibrium (2.5). The first step is to rewrite the equilibrium state (2.5) as

$$\eta + \phi = C, \qquad \text{where} \qquad \eta(p, \rho) = \frac{p}{\rho} \log \rho, \tag{3.27}$$

where C is a constant. The new variable η is the analogue of h in the case of polytropic equilibrium. Following the previous procedure, we can construct the equilibrium component of $\eta(x)$, denoted by $\eta^e(x)$, in the same way as in (3.8), which leads to the equilibrium component of the density, velocity, and pressure as follows:

$$\begin{aligned} \rho^e(x) &= \exp\left(\frac{\eta}{RT_0}\right), \\ p^e(x) &= RT_0 \exp\left(\frac{\eta}{RT_0}\right), \\ u^e(x) &= 0, \end{aligned} \tag{3.28}$$

the analogue of (3.9) in the case of polytropic equilibrium. If the constant temperature T_0 is not explicitly given, we can replace it by the average of temperature at the current time level t^n. From now on, the exact same approach to construct well-balanced numerical flux and source term approximation can be applied, and these will lead to well-balanced DG methods for the isothermal equilibrium (2.8) (or the equivalent form (3.27)). To save space, we do not repeat all these steps here.

4. Extension to multi-dimensional case

The one-dimensional well-balanced techniques presented in the previous section can be easily extended to multi dimensions. In this section, we discuss well-balanced DG methods for multi-dimensional Euler equations (1.1) with the gravitational field ϕ. The polytropic equilibrium is given by

$$\mathbf{u} = 0, \quad h + \phi = C, \tag{4.1}$$

or equivalently

$$\rho = \left(\frac{\gamma-1}{K\gamma}h\right)^{\frac{1}{\gamma-1}}, \qquad \mathbf{u} = 0, \qquad p = \frac{1}{K^{\frac{1}{\gamma-1}}}\left(\frac{\gamma-1}{\gamma}h\right)^{\frac{\gamma}{\gamma-1}}, \tag{4.2}$$

where $h = e + p/\rho$ denotes the specific enthalpy.

Consider the computational domain Ω, let $\mathcal{T}_\tau$ be a family of partitions parameterized by $\tau > 0$. For any element $K \in \mathcal{T}_\tau$, we define $\tau_K := \mathrm{diam}(K)$ and $\tau := \max_{K\in\mathcal{T}_\tau} \tau_K$. For each edge e_K^i $(i = 1, 2, \cdots)$ of K, we denote the outward unit normal vector by ν_K^i and the area of the triangle K by $|K|$.

For the ease of presentation, let us denote the multi-dimensional Euler equations (1.1) by

$$U_t + \nabla \cdot \mathbf{F}(U) = S(U, \phi),$$

where $U = (\rho, \rho\mathbf{u}, E)^T$, $\mathbf{F}(U)$ is the flux and S is the source term. The DG solution U_τ belongs to the finite dimensional piecewise polynomial space defined as

$$V_\tau^k \equiv \{w \in L^2(\Omega);\ w|_K \in Q^k(K),\ \ \forall K \in \mathcal{T}_\tau\}, \tag{4.3}$$

where $Q^k(K)$ denotes the space of tensor products of one-dimensional polynomials of degree up to k. The standard (non-well-balanced) semi-discrete DG method then takes the form of

$$\iint_K \partial_t U_\tau\, w\, \mathrm{d}\mathbf{x} - \int_K \mathbf{F}(U_\tau)\cdot\nabla w\, \mathrm{d}\mathbf{x} + \sum_{i=1}^m \int_{e_K^i} \widehat{\mathbf{F}}|_{e_K^i}\cdot\nu_K^i\, w\, \mathrm{d}s = \int_K S(U_\tau, \phi_\tau) w\, \mathrm{d}\mathbf{x}, \tag{4.4}$$

where $w(\mathbf{x})$ is a test function in the space V_τ^k. The numerical flux $\widehat{\mathbf{F}}$ is defined by

$$\widehat{\mathbf{F}}|_{e_K^i}\cdot\nu_K^i = \mathcal{F}(U_{\tau,i}^{int(K)}, U_{\tau,i}^{ext(K)}, \nu_K^i), \tag{4.5}$$

where $U_{\tau,i}^{int(K)}$ and $U_{\tau,i}^{ext(K)}$ are the approximations to the values on the edge e_K^i obtained from the interior and the exterior of K. For example, the simple global Lax–Friedrichs flux is given by

$$\mathcal{F}(a_1, a_2, \nu) = \frac{1}{2}\left[\mathbf{F}(a_1)\cdot\nu + \mathbf{F}(a_2)\cdot\nu - \alpha(a_2 - a_1)\right], \tag{4.6}$$

which satisfies the conservativity and consistency

$$\mathcal{F}(a_1, a_2, \nu) = -\mathcal{F}(a_2, a_1, -\nu), \quad \mathcal{F}(a_1, a_1, \nu) = \mathbf{F}(a_1)\cdot\nu. \tag{4.7}$$

In order to achieve the well-balanced property in multi space dimensions, we are interested in preserving the steady state solution (4.1) exactly, which can be achieved by extending the well-balanced techniques designed in section 3. Following the steps in one-dimensional case, we first introduce the special projection $\mathbf{P}_\tau^c$, defined as the tensor product of the one dimensional projections $\mathbb{P}_\tau^c$. We then define the initial condition $U_{0,\tau}$, and the projection of gravitational potential $\phi_\tau(x)$, to be

$$U_{0,\tau}(\mathbf{x}) = \mathbf{P}_\tau^c U_0(\mathbf{x}), \qquad \phi_\tau(\mathbf{x}) = \mathbf{P}_\tau^c \phi(\mathbf{x}), \tag{4.8}$$

which satisfy that

$$h(p_\tau(\mathbf{x}_K),\ \rho_\tau(\mathbf{x}_K)) + \phi_\tau(\mathbf{x}_K) = C, \qquad \text{for all elements } K, \tag{4.9}$$

where $\mathbf{x}_K$ denotes the center of the element K. Similarly, at each time step, we first define the equilibrium component of the specific enthalpy $h^e(x)$ as

$$h^e(\mathbf{x}) = h(p_\tau(\mathbf{x}_K),\ \rho_\tau(\mathbf{x}_K)) + \phi_\tau(\mathbf{x}_K) - \phi(\mathbf{x}), \tag{4.10}$$

and obtain the equilibrium component of the density, velocity, and pressure as follows:

$$\begin{aligned} \rho^e(\mathbf{x}) &= \left(\tfrac{1}{K}\tfrac{\gamma-1}{\gamma} h^e(\mathbf{x})\right)^{\frac{1}{\gamma-1}}, \\ p^e(\mathbf{x}) &= \left(\tfrac{1}{K}\right)^{\frac{1}{\gamma-1}} \left(\tfrac{\gamma-1}{\gamma} h^e(\mathbf{x})\right)^{\frac{\gamma}{\gamma-1}}, \\ \mathbf{u}^e(\mathbf{x}) &= 0. \end{aligned} \tag{4.11}$$

Then we can compute the equilibrium functions $U^e(x)$ from them, and use the same projection $\mathbf{P}_\tau^c$ to project them into the piecewise polynomial space V_τ^k by:

$$U_\tau^e(x) = \mathbf{P}_\tau^c U^e. \tag{4.12}$$

Therefore, we can decompose the DG solution U_τ into the reference equilibrium state U_τ^e and the remaining part U_τ^r as follows:

$$U_\tau = U_\tau^e + U_\tau^r. \tag{4.13}$$

As in the one dimensional case, the semi-discrete well-balanced DG methods, modified from the standard version (4.4), are defined as follows:

$$\iint_K \partial_t U_\tau\, w\, \mathrm{d}\mathbf{x} - \iint_K \mathbf{F}(U_\tau)\cdot\nabla w\, \mathrm{d}\mathbf{x} + \sum_{i=1}^m \int_{e_K^i} \widehat{\mathbf{F}}^*|_{e_K^i}\cdot \nu_K^i\, w\, \mathrm{d}s = \iint_K s(h,b)\, w\, \mathrm{d}\mathbf{x}. \tag{4.14}$$

The well-balanced numerical flux $\widehat{\mathbf{F}}^*$ is computed based on the hydrostatic reconstruction technique as follows. At each time step t^n, after computing the boundary values $U_{\tau,i}^{int(K)}$ and $U_{\tau,i}^{ext(K)}$ on the edge e_K^i, we first evaluate the updated boundary value, denoted by $U_{\tau,i}^{*,int(K)}$ and $U_{\tau,i}^{*,ext(K)}$, in a way analogous to (3.16) in the one dimensional case. The well-balanced numerical flux $\widehat{\mathbf{F}}^*$ is then given by:

$$\widehat{\mathbf{F}}^*|_{e_K^i}\cdot\nu_K^i = \mathcal{F}(U_{\tau,i}^{*,int(K)}, U_{\tau,i}^{*,ext(K)}, \nu_K^i) + \left(\mathbf{F}(U_{\tau,i}^{int(K)}) - \mathbf{F}(U_{\tau,i}^{*,int(K)})\right)\cdot\nu_K^i.$$

Following the derivation in section 3.4, the well-balanced approximation to the source term is given by:

$$\begin{aligned} &\iint_K S(U_\tau,\phi_\tau)\, w\, \mathrm{d}\mathbf{x} \\ &\quad\approx -\iint_K \mathbf{F}(U_\tau^e)\cdot\nabla w\, \mathrm{d}\mathbf{x} + \sum_{i=1}^m \int_{e_K^i} F(U_{\tau,i}^{e,int(K)})\cdot\nu_K^i\, w\, \mathrm{d}s + \iint_K S(U_\tau^r,\phi_\tau)\, w\, \mathrm{d}\mathbf{x}. \end{aligned}$$

Again, for the source term $-\iint_K (\rho\mathbf{u})_\tau\cdot\nabla\phi_\tau\, w\, \mathrm{d}\mathbf{x}$ which becomes zero at the equilibrium state, we can also apply the Gaussian quadrature rule with enough accuracy directly. Due to the fact that $\mathbf{u}_\tau^e = 0$, the approximation to the other source term takes the simplified form of

$$-\iint_K \rho_\tau\nabla\phi_\tau\, w\, \mathrm{d}\mathbf{x} \approx \sum_{i=1}^m \int_{e_K^i} p_{\tau,i}^{e,int(K)} w^{int(K)} \nu_K^i\, \mathrm{d}s - \iint_K p_\tau^e \nabla w\, \mathrm{d}\mathbf{x} - \iint_K \rho_\tau^r \nabla\phi_\tau\, w\, \mathrm{d}\mathbf{x}. \tag{4.15}$$

Table 1
L^1 errors and numerical orders of accuracy for the test case of Section 5.1.

N	ρ		ρu		E	
	L^1 error	Order	L^1 error	Order	L^1 error	Order
50	8.41E−03		1.47E−02		6.51E−02	
100	2.38E−03	1.82	4.40E−03	1.74	1.82E−02	1.84
200	4.42E−04	2.43	7.01E−04	2.65	2.88E−03	2.66
400	6.44E−05	2.78	9.99E−05	2.81	3.94E−04	2.87
800	8.56E−06	2.91	1.29E−05	2.95	5.20E−05	2.92
1600	1.06E−06	3.01	1.64E−06	2.98	6.41E−06	3.02

The fully discretized method can be obtained by combining with high order TVD Runge–Kutta methods. All the desired properties proved in the one-dimensional case, such as high order accuracy and the well-balanced property, are still valid in the multi-dimensional case.

Remark 4. If the finite dimensional piecewise polynomial space is defined as

$$V_\tau^k \equiv \{w \in L^2(\Omega);\ w|_K \in P^k(K),\ \ \forall K \in \mathcal{T}_\tau\}, \tag{4.16}$$

where $P^k(K)$ denotes the space of polynomials on the element K with at most k-th degree, the initial projection $\mathbf{P}_\tau^c$ can no longer be defined in this way. Under this circumstance, we can replace this special projection by the standard L^2 projection as in one-dimensional case, and observe numerically that the relation (4.9) holds with a round-off error.

5. Numerical results

In this section, we carry out extensive one- and two-dimensional numerical experiments to demonstrate the performance of the proposed well-balanced DG methods. In all the computations, we use the third order TVD Runge–Kutta methods (3.24), coupled with third order finite element DG methods (i.e., $k = 2$). The CFL number is taken as 0.18.

5.1. Accuracy test

The accuracy of the proposed DG methods is tested in this example. In analogy to [6], we take the following initial data

$$\rho(x,0) = \exp(-x), \quad u(x,0) = 0, \quad p(x,0) = (1+x)\exp(-x),$$

coupled with $\phi(x) = x$ as well as $\gamma = 1.4$ on a unit domain $[0,1]$. We compute this example up to $t = 0.1$, and use a much refined mesh of 6400 cells to compute a reference exact solution. The numerical errors and the order of accuracy are demonstrated in Table 1. It is obvious to observe that the expected high order accuracy is achieved by the proposed DG methods.

5.2. Hydrostatic atmosphere in a linear gravitational field

Next, we consider a very simple setup of polytropic hydrostatic atmosphere studied in [13]. Under a linear gravitational field $\phi(x) = gx$, the steady state solutions are given by

$$\begin{aligned} &\rho(x) = \left(\rho_0^{\gamma-1} - \tfrac{1}{K_0}\tfrac{\gamma-1}{\gamma} gx\right)^{\frac{1}{\gamma-1}}, \\ &p(x) = K_0\rho(x)^\gamma, \\ &u(x) = 0, \end{aligned} \tag{5.1}$$

with $g = 1$, $\gamma = 5/3$, $\rho_0 = 1$, $p_0 = 1$ and $K_0 = p_0/\rho_0^\gamma$ on a computational domain $[0, 2]$. In the following, we consider three different test cases, respectively.

5.2.1. Well-balanced property

We use the first example to test the well-balanced property of the proposed DG methods. The initial conditions are taken as the steady state solutions (5.1). In order to demonstrate that the steady state is indeed maintained up to the round-off error, we apply single precision and double precision respectively to carry out the computation. We compute this example up to $t = 4$ on meshes with both 100 and 200 uniform cells, and present the L^1 errors of numerical solutions in Table 2. We can clearly observe that the numerical errors are all at the level of round-off error for different precisions, which verify the desired well-balanced property accordingly.

Table 2
L^1 errors for different precisions for the steady state solutions in Section 5.2.1.

N	Precision	ρ	ρu	E
100	Single	7.02E−08	3.74E−07	1.75E−07
	Double	9.14E−15	4.98E−16	5.94E−16
200	Single	1.98E−07	6.69E−07	3.44E−07
	Double	7.42E−15	6.21E−15	7.08E−16

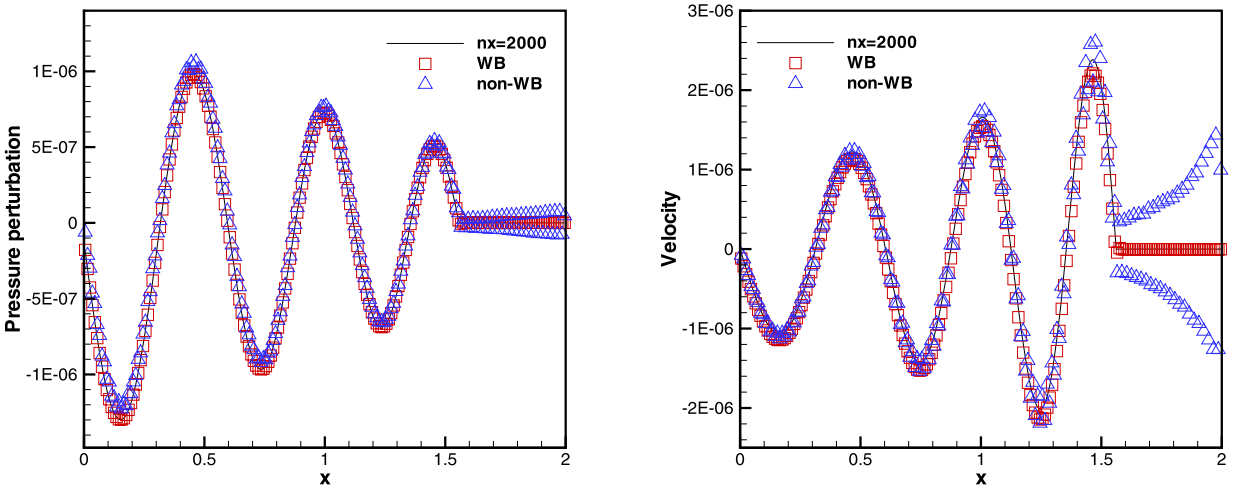

Fig. 1. Small amplitude wave propagation in Section 5.2.2. Numerical results by well-balanced DG methods with 200 and 2000 cells, and those by non-well-balanced (denoted by non-WB) DG methods with 200 cells at $t = 1.5$. Pressure perturbation (left) and velocity (right).

5.2.2. Small amplitude wave propagation

In this test, we impose a small perturbation to the equilibriums state, and compare the performance of well-balanced and non-well-balanced DG methods in capturing such small perturbation. A periodic velocity perturbation

$$u(x,t) = A\sin(4\pi t),$$

with $A = 10^{-6}$ is added to the system at the bottom of the atmosphere. We compute the solutions until $t = 1.5$, before the waves propagate to the upper boundary. The amplitude of the generated wave is modified by the density and pressure stratification as it moves through the domain.

In Fig. 1, we present the pressure perturbation and the velocity at $t = 1.5$ on a mesh with 200 cells against the reference solutions obtained with a much refined 2000 cells. Moreover, we run the same numerical test with non-well-balanced DG methods using a straightforward integration of the source term, and show their results in the same figure for the sake of comparison. Easy to observe that the results by the well-balanced DG methods are in good agreement with the reference solutions, while those by the non-well-balanced DG methods are not consistent with the reference solutions for $x > 1.5$. This observation indicates the importance of the well-balanced methods in capturing small amplitude perturbations to the equilibrium state.

5.2.3. Large amplitude wave propagation

At the end, we repeat the calculation with a large amplitude perturbation $A = 0.1$. We compute the solutions until $t = 1.5$, before the waves propagate to the upper boundary.

Both the numerical results by the well-balanced and non-well-balanced DG methods against the reference solutions are displayed in Fig. 2. The numerical results by both DG methods match well with the reference solutions for this large amplitude perturbation. This shows that, as expected, the well-balanced methods perform similarly as non-well-balanced methods when far away from the steady states. This large amplitude test shows that the hydrostatic reconstruction and non-trivial source term approximation introduced in this paper do not destroy the robustness of the DG methods for general solutions.

5.3. Contact discontinuity under gravitational field

In this example, we test an initial contact discontinuity wave under a linear gravitational field $\phi(x) = x$ as in [6]. The initial data are defined as follows:

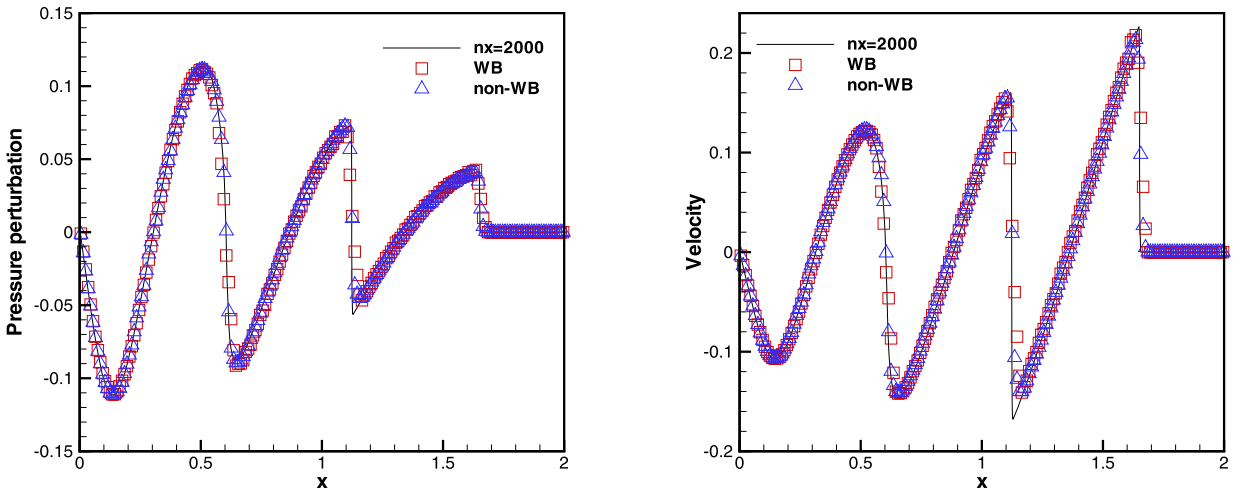

Fig. 2. Large amplitude wave propagation in Section 5.2.3. Numerical results by well-balanced DG methods with 200 and 2000 cells, and those by non-well-balanced (denoted by non-WB) DG methods with 200 cells at $t = 1.5$. Pressure perturbation (left) and velocity (right).

$$(\rho, u, p) = \begin{cases} (1, 0, 1) & \text{if } x < 0.5, \\ (10, 0, 1) & \text{otherwise,} \end{cases}$$

on a computational domain $[0, 1]$ with $\gamma = 1.4$. On both end points, we impose the solid wall boundary conditions. We present the numerical solutions at $t = 0.6$ on a mesh with 200 cells against the reference solutions obtained with 2000 cells in Fig. 3. In addition, we also show the numerical results by the non-well-balanced DG methods with a straightforward numerical discretization of the source term. We can easily observe a better performance of the well-balanced methods over the non-well-balanced ones.

5.4. Two-dimensional polytrope

As in [13,18], in this example, we consider a two-dimensional test case from the astrophysical problem. These model stars are constructed from the hydrostatic equilibrium:

$$\frac{\mathrm{d}p}{\mathrm{d}r} = -\rho \frac{\mathrm{d}\phi}{\mathrm{d}r}, \tag{5.2}$$

with $\gamma = 2$. This model has the following steady state

$$\rho(r) = \rho_c \frac{\sin(\alpha r)}{\alpha r}, \quad u(r) = 0, \quad v(r) = 0, \quad p(r) = K\rho(r)^2, \tag{5.3}$$

coupled with a given gravitational potential

$$\phi(r) = -2K\rho_c \frac{\sin(\alpha r)}{\alpha r}, \tag{5.4}$$

where $\alpha = \sqrt{\frac{4\pi g}{2K}}$ with $K = g = \rho_c = 1$ and $r = \sqrt{x^2 + y^2}$ being the radial variable. We refer to [13] for the detailed derivation of the steady state.

The computational domain is set as $[-0.5, 0.5] \times [-0.5, 0.5]$. In order to test the capability of the well-balanced methods in capturing small perturbations of the hydrostatic equilibrium and preserving the axial symmetry, we initially impose a small Gaussian hump perturbations in pressure to the steady state (5.3) as follows:

$$p(r) = K\rho(r)^2 + 0.001 \exp(-100r^2).$$

We evolved the solution up to $t = 0.2$ on a mesh with 100×100 uniform cells. The contour plots of the pressure perturbation and the velocity $\sqrt{u^2 + v^2}$ are presented in Figs. 4 and 5. From these figures, we can clearly observe that the non-well-balanced DG methods are not capable of capturing such small perturbation on the relatively coarse mesh, while the well-balanced ones can resolve it very well. Also, the well-balanced DG methods preserve the axial symmetry, but the non-well-balanced ones can not keep this symmetry well.

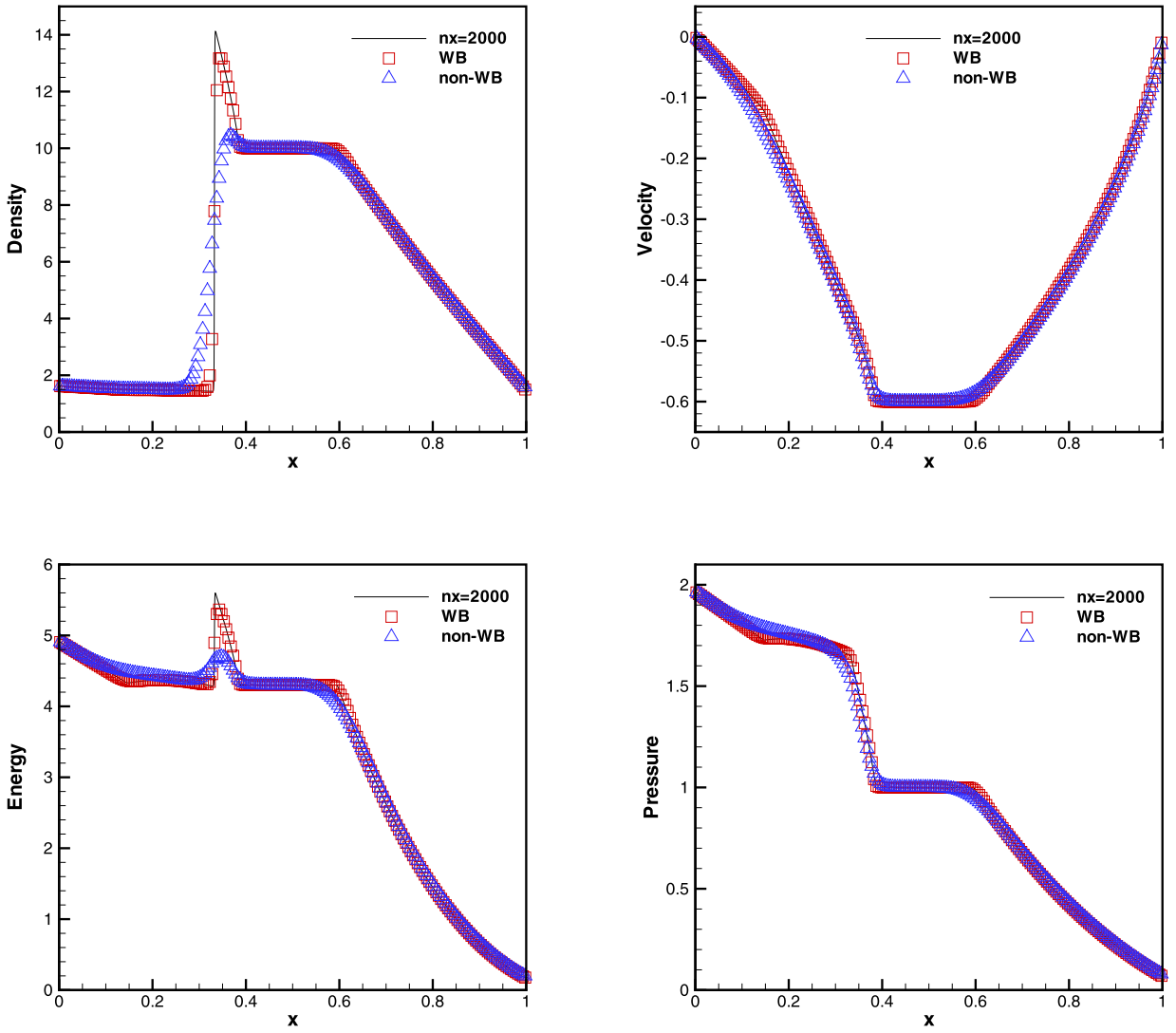

Fig. 3. Contact discontinuity under gravitational field in Section 5.3. Numerical results by well-balanced DG methods with 200 and 2000 cells, and those by non-well-balanced (denoted by non-WB) DG methods with 200 cells at $t = 0.6$. Top left: density; Top right: velocity; Bottom left: energy; Bottom right: pressure.

5.5. Polytropic hydrostatic solution

In the last test case, we consider a polytropic hydrostatic solution inspired by [6]

$$\rho_e(x, y) = (T_e(x, y))^{\frac{1}{\gamma-1}}, \quad u_e(x, y) = v_e(x, y) = 0, \quad p_e(x, y) = (T_e(x, y))^{\frac{\gamma}{\gamma-1}}, \tag{5.5}$$

on a unit domain $[0, 1] \times [0, 1]$ with $T_e(x, y) = 1 - \frac{\gamma-1}{\gamma}\phi(x, y)$, $\gamma = 1.4$, as well as $\phi(x, y) = x + y$.

5.5.1. Well-balanced property

We first test the well-balanced property of our proposed DG methods. Taking the equilibrium state (5.5) as the initial condition, we compute the solution up to $t = 0.5$ on meshes with 50×50 and 100×100 uniform cells. In order to demonstrate that the steady state is indeed maintained up to round-off error even on the coarse meshes, we use single precision and double precision respectively to carry out the computation. The L^1 errors of ρ, ρu, ρv and E are shown in Table 3, where the well-balanced property can be easily observed.

5.5.2. Perturbation to the polytropic hydrostatic solution

Subsequently, we impose a perturbation to the initial pressure state:

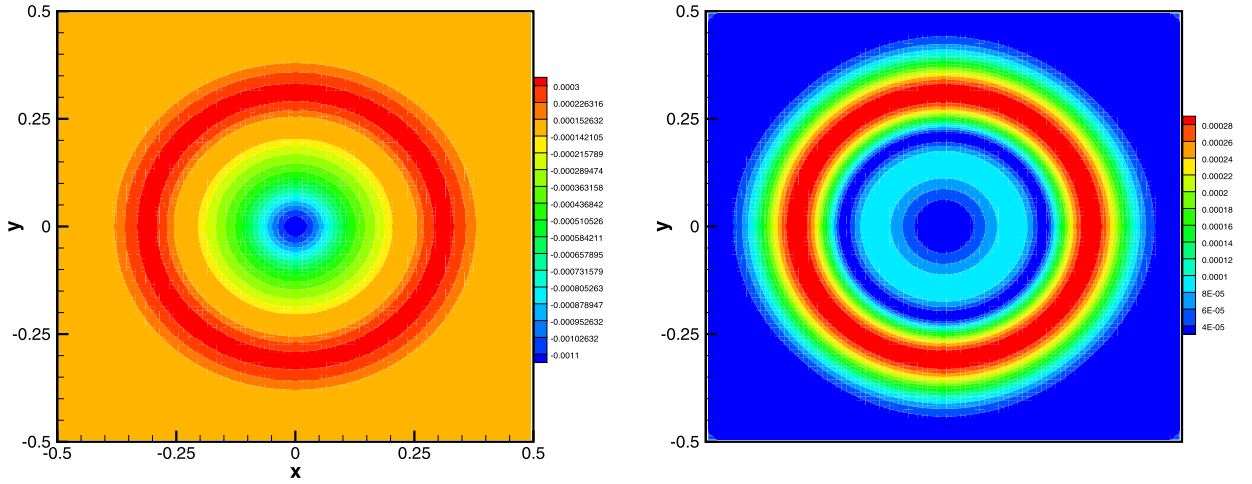

Fig. 4. Two-dimensional polytrope in Section 5.4. Contours of numerical results by well-balanced DG methods with 100×100 cells at $t = 0.2$. Left: pressure perturbation; Right: velocity $\left(\sqrt{u^2 + v^2}\right)$.

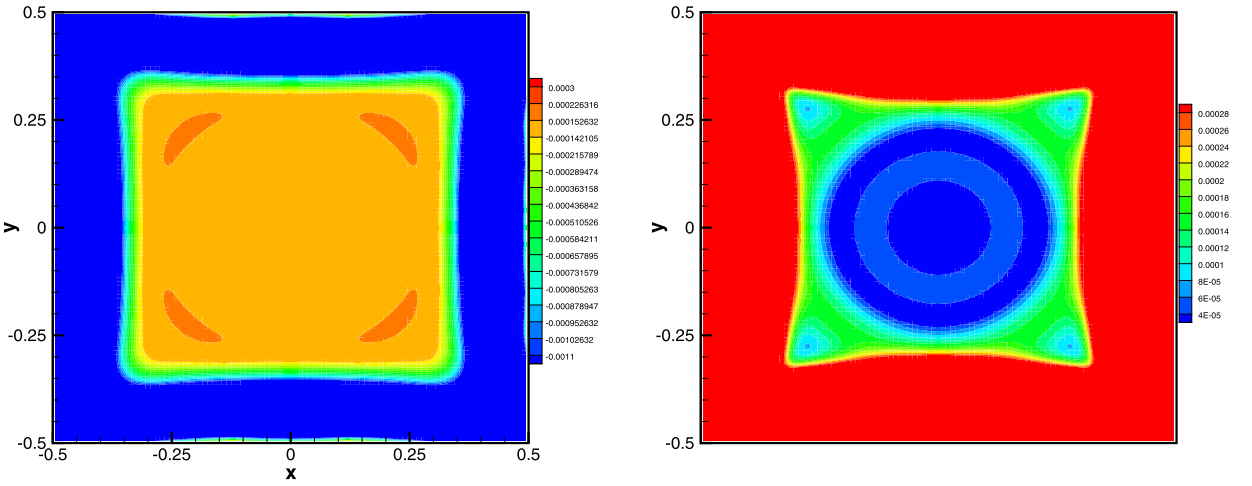

Fig. 5. Two-dimensional polytrope in Section 5.4. Contours of numerical results by non-well-balanced DG methods with 100×100 cells at $t = 0.2$. Left: pressure perturbation; Right: velocity $\left(\sqrt{u^2 + v^2}\right)$.

Table 3
L^1 errors for different precisions for the steady state solutions (5.5) in Section 5.5.1.

N	Precision	ρ	ρu	ρv	E
50×50	Single	7.95E−7	5.42E−7	4.32E−7	2.04E−7
	Double	6.20E−14	8.07E−14	8.07E−14	9.81E−14
100×100	Single	1.41E−6	9.42E−6	8.01E−7	3.61E−6
	Double	8.79E−14	1.10E−13	1.10E−13	5.15E−13

$$\rho(x, y, 0) = \rho_e(x, y)$$
$$u(x, y, 0) = 0,$$
$$v(x, y, 0) = 0,$$
$$p(x, y, 0) = p_e(x, y) + \eta \exp\left(-100\rho_0 g((x - 0.3)^2 + (y - 0.3)^2)/p_0\right),$$

with $g = 1$, $\rho_0 = 1.21$ and $p_0 = 1$. We show the numerical results with perturbation size $\eta = 0.1$ at $t = 0.15$ by both well-balanced and non-well-balanced DG methods in Figs. 6 and 7. It is evident that the numerical results by the well-balanced DG methods are with more resolution when compared with those by the non-well-balanced DG methods. Moreover, we reduce the size of the perturbation to $\eta = 0.001$ and repeat the simulation. The numerical results at $t = 0.15$ are shown in

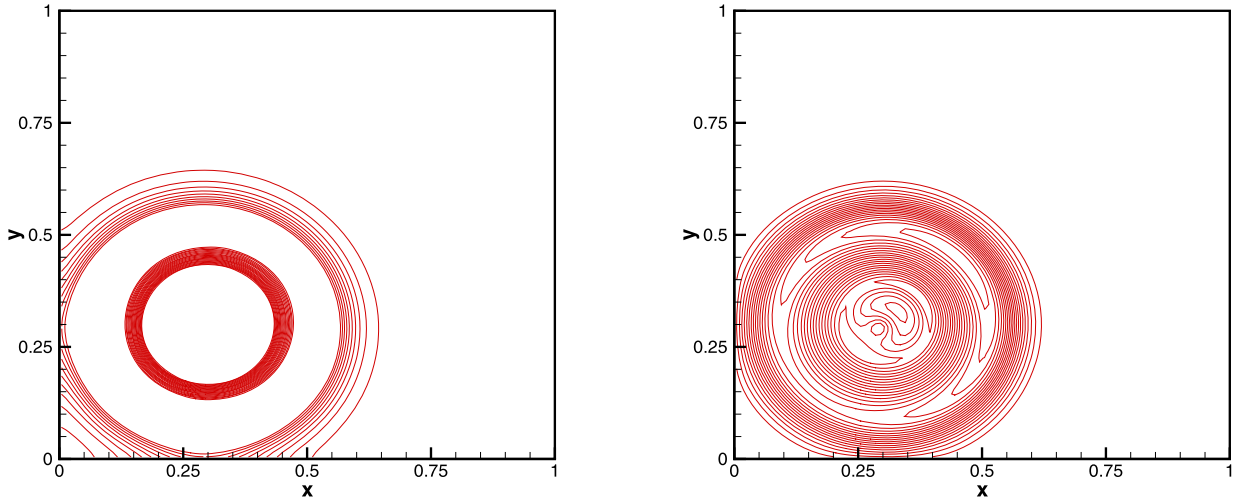

Fig. 6. Perturbation to the polytropic hydrostatic solution with $\eta = 0.1$ in Section 5.5.2. Contours of numerical results by well-balanced DG methods with 100×100 cells at $t = 0.15$. Left: twenty equally spaced contours between -0.03 and $+0.03$ of pressure perturbation. Right: twenty equally spaced contours between 0.01 and 0.12 of velocity $\left(\sqrt{u^2 + v^2}\right)$.

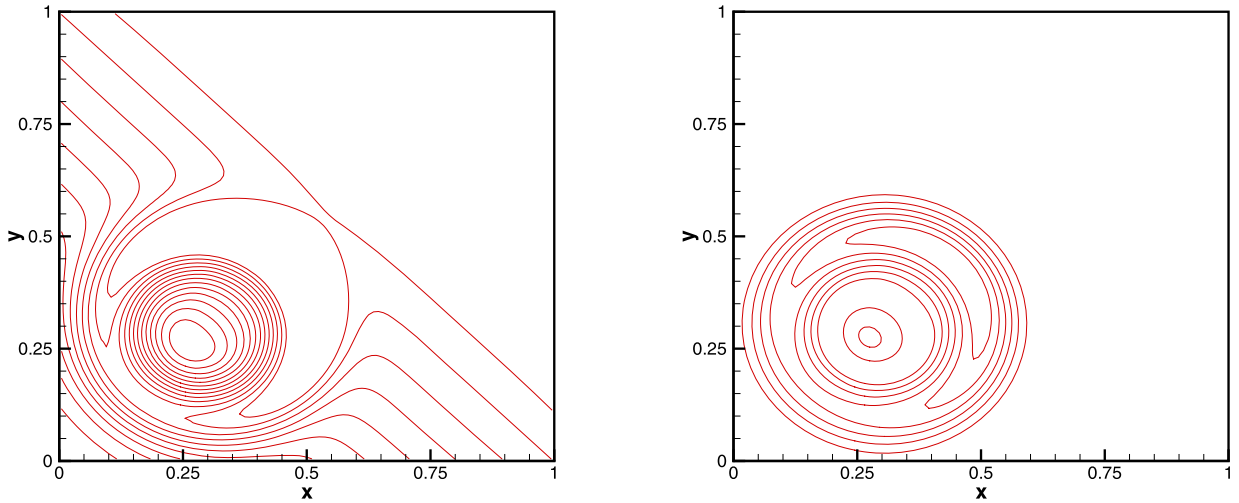

Fig. 7. Perturbation to the polytropic hydrostatic solution with $\eta = 0.1$ in Section 5.5.2. Contours of numerical results by non-well-balanced DG methods with 100×100 cells at $t = 0.15$. Left: twenty equally spaced contours between -0.03 and $+0.03$ of pressure perturbation. Right: twenty equally spaced contours between 0.01 and 0.12 of velocity $\left(\sqrt{u^2 + v^2}\right)$.

Figs. 8 and 9. Again, the well-balanced DG methods continue to produce numerical results with good resolution, while the non-well-balanced DG methods fail to capture the small perturbation thoroughly.

6. Concluding remarks

In this paper, we have constructed well-balanced DG methods for the polytropic and isothermal equilibrium state solutions of the Euler equations with gravitation. The idea of hydrostatic reconstruction is used to construct the well-balanced numerical flux. By combining it with a novel source term approximation, one can achieve the well-balanced property. Extensive one- and two-dimensional numerical examples are carried out to demonstrate the high order accuracy, well-balanced property, ability to capture small perturbation of the equilibrium state on relatively coarse meshes, and good resolution of the proposed numerical methods for both continuous and discontinuous solutions.

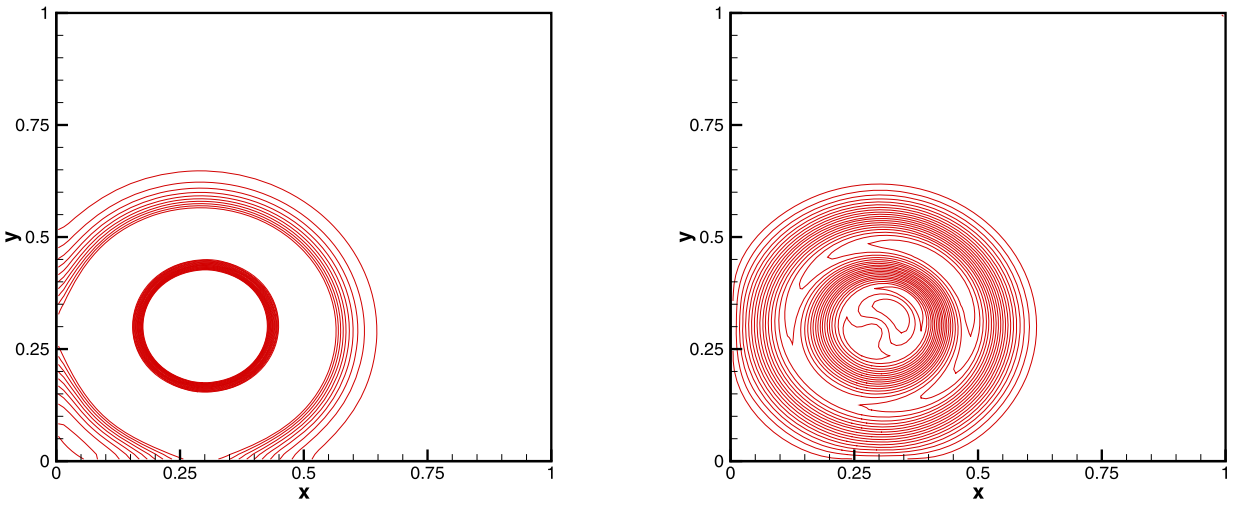

Fig. 8. Perturbation to the polytropic hydrostatic solution with $\eta = 0.001$ in Section 5.5.2. Contours of numerical results by well-balanced DG methods with 100×100 cells at $t = 0.15$. Left: twenty equally spaced contours between -0.00025 and $+0.00025$ of pressure perturbation. Right: twenty equally spaced contours between 0.0001 and 0.0014 of velocity $\left(\sqrt{u^2 + v^2}\right)$.

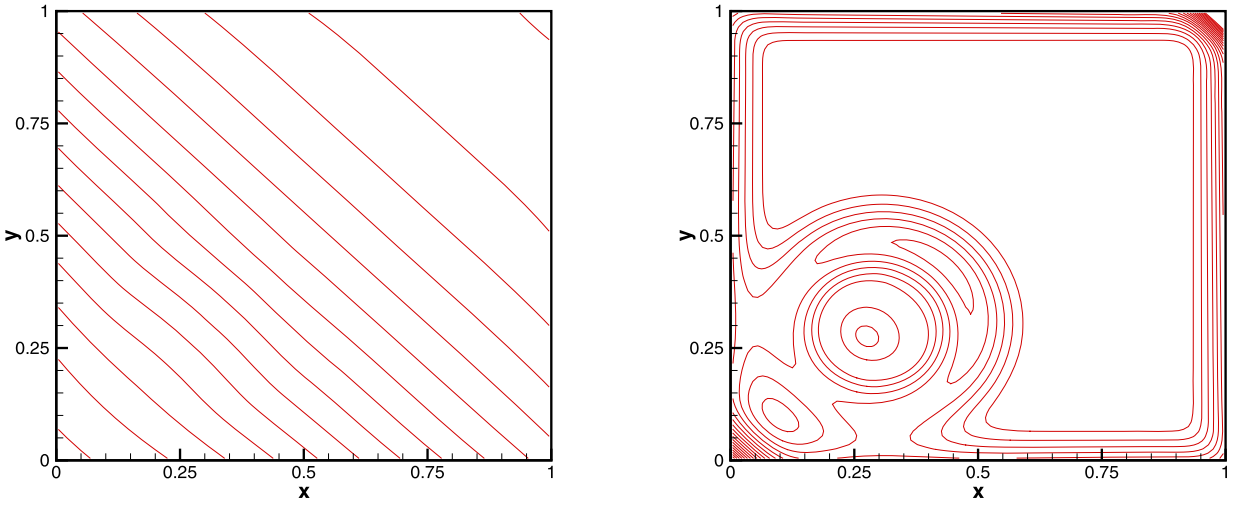

Fig. 9. Perturbation to the polytropic hydrostatic solution with $\eta = 0.001$ in Section 5.5.2. Contours of numerical results by non-well-balanced DG methods with 100×100 cells at $t = 0.15$. Left: twenty equally spaced contours between 0.006 and 0.025 of pressure perturbation. Right: twenty equally spaced contours between 0.0001 and 0.0014 of velocity $\left(\sqrt{u^2 + v^2}\right)$.

Acknowledgements

This work by the first author was partially performed at the State Key Laboratory of Science/Engineering Computing of P.R. China by virtue of the computational resources of Professor Li Yuan's group. The first author is also thankful to Professor Li Yuan for his kind invitation.

References

[1] E. Audusse, F. Bouchut, M.-O. Bristeau, R. Klein, B. Perthame, A fast and stable well-balanced scheme with hydrostatic reconstruction for shallow water flows, SIAM J. Sci. Comput. 25 (2004) 2050–2065.
[2] A. Bermudez, M.E. Vazquez, Upwind methods for hyperbolic conservation laws with source terms, Comput. Fluids 23 (1994) 1049–1071.
[3] N. Botta, R. Klein, S. Langenberg, S. Lützenkirchen, Well-balanced finite volume methods for nearly hydrostatic flows, J. Comput. Phys. 196 (2004) 539–565.
[4] F. Bouchut, T. Morales, A subsonic-well-balanced reconstruction scheme for shallow water flows, SIAM J. Numer. Anal. 48 (2010) 1733–1758.
[5] M.J. Castro, A. Pardo Milanes, C. Pares, Well-balanced numerical schemes based on a generalized hydrostatic reconstruction technique, Math. Models Methods Appl. Sci. 17 (2007) 2055–2113.

[6] P. Chandrashekar, C. Klingenberg, A second order well-balanced finite volume scheme for Euler equations with gravity, SIAM J. Sci. Comput. 37 (2015) 382–402.
[7] P. Chandrashekar, M. Zenk, Well-balanced nodal discontinuous Galerkin method for Euler equations with gravity, J. Sci. Comput. 71 (2017) 1062–1093.
[8] P. Ciarlet, The Finite Element Method for Elliptic Problem, North-Holland, 1978.
[9] B. Cockburn, C.-W. Shu, The Runge–Kutta discontinuous Galerkin method for conservation laws V: multidimensional systems, J. Comput. Phys. 141 (1998) 199–224.
[10] V. Desveaux, M. Zenk, C. Berthon, C. Klingenberg, A well-balanced scheme for the Euler equation with a gravitational potential, in: Finite Volumes for Complex Applications VII—Methods and Theoretical Aspects, in: Springer Proceedings in Mathematics & Statistics, vol. 77, 2014, pp. 217–226.
[11] D. Ghosh, E.M. Constantinescu, A well-balanced, conservative finite difference algorithm for atmospheric flows, AIAA J. 54 (2016) 1370–1385.
[12] J.M. Greenberg, A.Y. LeRoux, A well-balanced scheme for the numerical processing of source terms in hyperbolic equations, SIAM J. Numer. Anal. 33 (1996) 1–16.
[13] R. Käppeli, S. Mishra, Well-balanced schemes for the Euler equations with gravitation, J. Comput. Phys. 259 (2014) 199–219.
[14] R. Käppeli, S. Mishra, A well-balanced finite volume scheme for the Euler equations with gravitation. The exact preservation of hydrostatic equilibrium with arbitrary entropy stratification, Astron. Astrophys. 587 (2016) A94.
[15] R.J. LeVeque, Balancing source terms and flux gradients on high-resolution Godunov methods: the quasi-steady wave-propagation algorithm, J. Comput. Phys. 146 (1998) 346–365.
[16] R.J. LeVeque, D.S. Bale, Wave propagation methods for conservation laws with source terms, in: Proceedings of the 7th International Conference on Hyperbolic Problems, 1998, pp. 609–618.
[17] G. Li, Y. Xing, Well-balanced discontinuous Galerkin methods for the Euler equations under gravitational fields, J. Sci. Comput. 67 (2016) 493–513.
[18] G. Li, Y. Xing, High order finite volume WENO schemes for the Euler equations under gravitational fields, J. Comput. Phys. 316 (2016) 145–163.
[19] J. Luo, K. Xu, N. Liu, A well-balanced symplecticity-preserving gas-kinetic scheme for hydrodynamic equations under gravitational field, SIAM J. Sci. Comput. 33 (2011) 2356–2381.
[20] S. Noelle, Y. Xing, C.-W. Shu, High-order well-balanced finite volume WENO schemes for shallow water equation with moving water, J. Comput. Phys. 226 (2007) 29–58.
[21] B. Perthame, C. Simeoni, A kinetic scheme for the Saint-Venant system with a source term, Calcolo 38 (2001) 201–231.
[22] C.-W. Shu, TVB uniformly high-order schemes for conservation laws, Math. Comput. 49 (1987) 105–121.
[23] C.-W. Shu, Total-variation-diminishing time discretizations, SIAM J. Sci. Stat. Comput. 9 (1988) 1073–1084.
[24] C.T. Tian, K. Xu, K.L. Chan, L.C. Deng, A three-dimensional multidimensional gas-kinetic scheme for the Navier–Stokes equations under gravitational fields, J. Comput. Phys. 226 (2007) 2003–2027.
[25] Y. Xing, Exactly well-balanced discontinuous Galerkin methods for the shallow water equations with moving water equilibrium, J. Comput. Phys. 257 (2014) 536–553.
[26] Y. Xing, C.-W. Shu, High order finite difference WENO schemes with the exact conservation property for the shallow water equations, J. Comput. Phys. 208 (2005) 206–227.
[27] Y. Xing, C.-W. Shu, A new approach of high order well-balanced finite volume WENO schemes and discontinuous Galerkin methods for a class of hyperbolic systems with source terms, Commun. Comput. Phys. 1 (2006) 100–134.
[28] Y. Xing, C.-W. Shu, High order well-balanced WENO scheme for the gas dynamics equations under gravitational fields, J. Sci. Comput. 54 (2013) 645–662.
[29] Y. Xing, C.-W. Shu, A survey of high order schemes for the shallow water equations, J. Math. Study 47 (2014) 221–249.
[30] Y. Xing, X. Zhang, C.-W. Shu, Positivity-preserving high order well-balanced discontinuous Galerkin methods for the shallow water equations, Adv. Water Resour. 33 (2010) 1476–1493.
[31] K. Xu, A well-balanced gas-kinetic scheme for the shallow-water equations with source terms, J. Comput. Phys. 178 (2002) 533–562.
[32] K. Xu, J. Luo, S. Chen, A well-balanced kinetic scheme for gas dynamic equations under gravitational field, Adv. Appl. Math. Mech. 2 (2010) 200–210.
[33] M. Zingale, L.J. Dursi, J. ZuHone, A.C. Calder, B. Fryxell, T. Plewa, J.W. Truran, A. Caceres, K. Olson, P.M. Ricker, K. Riley, R. Rosner, A. Siegel, F.X. Timmes, N. Vladimirova, Mapping initial hydrostatic models in Godunov codes, Astrophys. J. Suppl. Ser. 143 (2002) 539–565.